Polymer 51 (2010) 5400–5406

Contents lists available at ScienceDirect

Polymer

journal homepage: www.elsevier.com/locate/polymer

Shape-controlled fabrication of polypyrrole microstructures by replicating organic crystals through electrostatic interactions

Sang Soo Jeon [a], Chong Seung Yoon [b], Seung Soon Im [a,*]

[a] Department of Fiber and Polymer Engineering, Hanyang University, Seoul 133-791, Republic of Korea
[b] Division of Materials Science and Engineering, Hanyang University, Seoul 133-791, Republic of Korea

ARTICLE INFO

Article history:
Received 29 July 2010
Received in revised form
6 September 2010
Accepted 14 September 2010
Available online 21 September 2010

Keywords:
Polypyrrole
Organic crystal
Template

ABSTRACT

Polypyrrole (PPy) microstructures with diverse shapes were synthesized in an aqueous inorganic salt medium including organic crystals and pyrrole (Py). A series of sulfobenzoic acid salt forms with various cations (K^+, Na^+, Li^+, NH_4^+) in different positions (*para*, *meta*, *ortho*) of the sulfonate group on the benzene ring were used to form organic crystals as sacrificial templates. Using these crystals, we produced five different shapes of PPy microstructures (hexagonal microplates, curled nanofibers, lozenge-shaped microplates, rigid rods, parallelogram microplates), which replicated the shapes of the organic crystal templates through electrostatic interaction between the anionic crystal surfaces and the cationic PPy chains. In contrast, PPy that was polymerized without crystals showed bulky agglomerates of 200–500 nm size. The electrical properties were dictated by the molecular structures of the organic salt molecules used. While the highest conductivity (200.3 Scm^{-1}) was observed in PPy using crystals of *para*-linked 4-sulfobenzoic acid monopotassium salt, the lowest conductivity (0.8 Scm^{-1}) was observed in PPy prepared in the presence of crystals of *ortho*-linked 2-sulfobenzoic acid monoammonium salt.

1. Introduction

Various synthetic routes for conducting polymers have been developed, both chemically and electrochemically, for fabricating the micro/nanostructures. Among these methods, hard [1–3] and soft template [4–12] methods have been used to prepare micro/nanostructured conducting polymers in a controlled manner. These methods have successfully provided morphologically well-defined micro/nanostructures from zero-dimensional nanoparticles and microspheres to one-dimensional nanofibers and nanotubes with small diameters (<100 nm) and micrometer lengths. Such well-defined conducting polymer micro/nanostructures with highly controlled properties could extend the application area of conducting polymers in plastic electronics.

Despite the many different synthetic routes to conducting polymer micro/nanostructures, however, preparing uniform-sized and -shaped micro/nanostructures from conducting polymers in a practical, cost-effective way still remains a challenge. Recently, it was reported that various complexes of organic dopant/oxidant, organic dopant/monomer, or organic dopant/fluorosurfactant could be used as templates for fabrication of conducting polymer nano/micro structures [13–15]. Dai et al. successfully fabricated the conducting polymer microtubes using methyl orange fibrils formed in HCl solution as templates [16]. In addition, Wang et al. reported the chemical synthesis of spiral nanostructures of polypyrrole (PPy) and polyaniline (PANI) using a hydrated crystallite of surfactant as a template [17,18]. More recently, for the first time, we developed an organic single-crystal surface-induced fabrication method capable of producing PPy micro-hexagonal plates with an improved structural order and high conductivity (~400 Scm^{-1}) [19]. This method relies on a shape-copying process based on electrostatic interactions between anionic organic crystal surfaces and cationic PPy chains.

Here, we report a general strategy for fabricating diverse types of conducting PPy microstructures using crystals of organic salt molecules, 4-sulfobenzoic acid monopotassium salt (4-SBAK), 4-sulfobenzoic acid monosodium salt (4-SBANa), 4-sulfobenzoic acid monolithium salt (4-SBALi), 3-sulfobenzoic acid monosodium salt (3-SBANa), and 2-sulfobenzoic acid monoammonium salt (2-$SBANH_4$), as sacrificial templates. Using these organic crystals, we produced five different shapes of PPy microstructures, dictated by the shapes of the template organic crystals. Different from the previous reports, in our method, only the crystals of organic salt molecules were used as sacrificial templates for inducing the shape-copying process. The organic crystals were formed at zero or sub-zero temperature by rapid injection of organic salt solution

* Corresponding author. Tel.: +82 2 2220 0495; fax: +82 2 2297 5859.
E-mail address: imss007@hanyang.ac.kr (S.S. Im).

0032-3861/$ – see front matter © 2010 Elsevier Ltd. All rights reserved.
doi:10.1016/j.polymer.2010.09.032

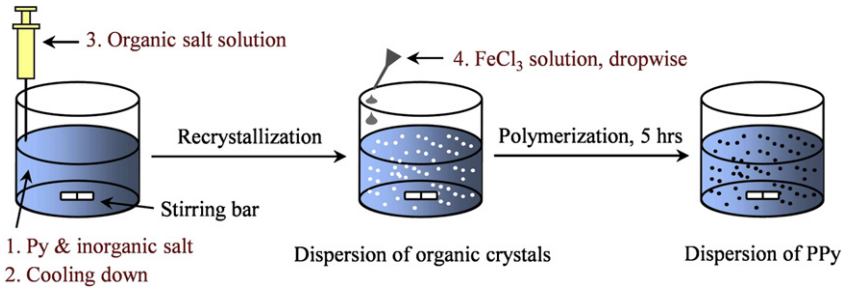

Fig. 1. Polymerization scheme of the PPy microstructues by replicating organic crystals.

into a nearly saturated solution of inorganic salt containing counter cations of the organic salt to prevent cation exchange between inorganic and organic salts. Inorganic salts, KCl, NaCl, LiCl, and NH_4Cl used in the experiment also lowered the freezing temperature of polymerization medium and decreased the solubility of organic salt molecules to facilitate the formation of the organic crystals. We systematically investigated the effect of different cations and different positions (*para*, *meta* and *ortho*) of the sulfonate group on the benzene ring on the morphologies of crystals and electrical properties of their replicated PPys. Wide-angle X-ray diffraction (WAXD), optical microscopy (OM), and scanning electron microscopy (SEM) analyses were conducted to confirm the morphology and formation mechanism of the PPy microstructures.

2. Experimental

2.1. Materials

Pyrrole (Py) (Sigma–Aldrich, 99%) was vacuum-distilled and stored at 2 °C. The oxidant, $FeCl_3$ (Riedel, 98%), was used without further purification. 4-SBAK (Sigma–Aldrich, 95%), 4-SBANa (Sigma–Aldrich, 95%), 4-SBALi (Sigma–Aldrich, 95%), 3-SBANa (Sigma–Aldrich, 97%), and 2-$SBANH_4$ (Tokyo Kasei) were purified by recrystallization in water and acetone. Inorganic salts, such as KCl (Sigma–Aldrich, 99%), NaCl (Sigma–Aldrich, >98%), LiCl (Sigma–Aldrich, 99%), and NH_4Cl (Sigma–Aldrich, 99.5%), were used as received.

2.2. Synthesis

A typical synthesis proceeded as follows. Py dissolved in 100 mL of aqueous inorganic salt solution, while the organic salt, 4-SBAK, 4-SBANa, 4-SBALi, 3-SBANa, or 2-$SBANH_4$, dissolved in 10 mL of water. The above monomeric solution was cooled to 0 or −10 °C, and then the organic salt solution was injected quickly with vigorous stirring. To prevent cation exchange between inorganic and organic salts, an inorganic salt containing the same cation as the organic salt was used in all reactions (*e.g.*, 4-SBAK solution in KCl solution and 4-SBANa solution in NaCl solution). A white organic crystal precipitates appeared immediately in the transparent mixture solution. $FeCl_3$ aqueous solution (20 mL) was added dropwise to the mixture. The white mixture gradually turned black. After 5 h, the PPys were filtered and washed with distilled water and acetone several times, and then dried in a vacuum oven at 60 °C for 24 h. The polymerization procedure of the PPy microstructures, by replicating organic crystals, is described in Fig. 1. Because the crystallization conditions of various organic salt molecules were different from each other, polymerization temperature and the concentrations of added organic salt and inorganic salt were set differently in each experiment. A conventional PPy sample was polymerized using the same procedure in the absence of organic salts. Details of the experimental recipes are presented in Table 1.

2.3. Characterization

The morphology of the organic crystals was observed by OM (Olympus BX-51) equipped with a charged coupled device (CCD) camera. The morphology of the synthesized PPys was observed by SEM (JEOL JSM6340). A zeta potential analyzer (Malvern model Zetasizer Nano-ZS) was used to measure the zeta potentials of the organic crystals and PPy dispersions at 20 °C. The dispersions were diluted with ethanol to 1.0 wt% before measurement. Fourier-transform infrared (FT-IR) spectra of the PPys in attenuated total reflection (ATR) mode were recorded on a PerkinElmer Spectrum 100 FT-IR spectrometer. The electrical conductivity (298 K) of a pressed pellet of the dried PPys was measured using the four-point probe method, with a Jandel contact-probe connected to a Keithley 238 high-current source-measuring unit. The conductivity data in Table 1 were measured from three independent samples of a single synthesis. WAXD measurements were carried out using a Rigaku Denki X-ray generator (D/MAX-2500) with CuKα radiation (λ = 1.5418 Å), operated at 40 kV and 100 mA. The bulk current–voltage (I–V) measurements were conducted using a conventional two-probe method. The probes were made of platinum and the distance between the two probes was maintained at 1.0 cm. The voltage was varied using a Keithley 2400 source-meter. X-ray photoelectron spectroscopy (XPS) measurements were performed using a Sigma Probe (Thermo VG, UK) system

Table 1
Polymerization recipe and yield of the PPy samples.

Sample	Pyrrole (mole)	Organic salt (mole)	Inorganic salt (mole)	Oxidant (mole)	Temperature (°C)	Yield[a] (%)
PPy-4SBAK	0.015	0.005	KCl (0.3)	0.03	0	47.3
PPy-4SBANa	0.015	0.005	NaCl (0.3)	0.03	0	49.1
PPy-4SBALi	0.015	0.008	LiCl (0.4)	0.03	0	45.7
PPy-3SBANa	0.015	0.005	NaCl (0.3)	0.03	−10	46.2
PPy-2$SBANH_4$	0.015	0.08	NH_4Cl (0.5)	0.03	−10	46.5
Conventional PPy	0.015		NaCl (0.3)	0.03	0	25.6

[a] Yield (%) = (weight of PPy/weight of Py monomer) ×100.

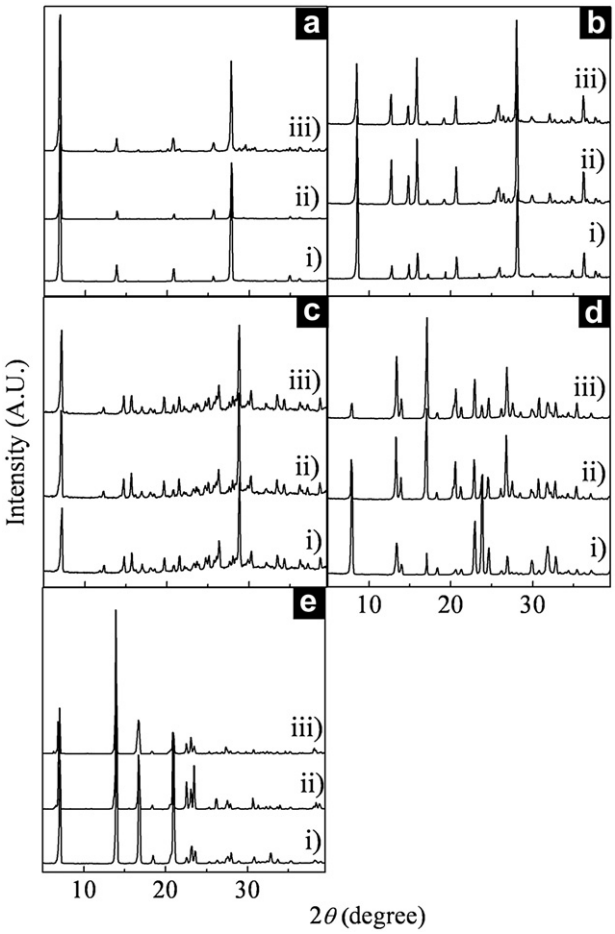

Fig. 2. XRD patterns of (a) 4-SBAK, (b) 4-SBANa, (c) 4-SBALi, (d) 3-SBANa, and (e) 2-$SBANH_4$ organic crystals. i) and ii) in each figure are XRD patterns of crystals that are precipitated in our polymerization medium before adding $FeCl_3$ and pure distilled water, respectively. iii) in each figure are XRD patterns of crystals that are filtered after adding $FeCl_3$ solution to organic crystal solution without Py.

equipped with a monochromatic AlKα X-ray source (1486.6 eV). The X-ray power supply was operated at 100 W (15 kV) and the X-ray spot size was 400 μm. All binding energies were referenced to a C 1s neutral carbon peak at 284.6 eV.

3. Results and discussion

Organic crystals could be formed simply by recrystallization from the respective aqueous inorganic salt solutions. Unlike our previous work [19], in the present study, inorganic salts such as KCl, NaCl, LiCl, and NH_4Cl, were used to lower the freezing point of the aqueous polymerization medium and expedite the recrystallization of the organic molecules by decreasing the solubility of the organic molecules in water. Fig. 2 shows the XRD patterns of organic crystals precipitated under various conditions. We observed that crystal structure of the organic crystals (curve i) in each figure) that are precipitated in the proposed polymerization medium before adding $FeCl_3$ were identical to the pure organic crystals (curve ii) in each figure) produced in only distilled water. This result indicates that once organic crystals were formed, they are very stable because Pys dissolved in the polymerization medium do not interact with the organic salt molecules and have no effect on the crystallization of the organic salt molecules under our polymerization conditions. We also confirmed that even after adding $FeCl_3$ to the organic crystal solution without Py, the crystal structure of the organic salts (curve iii) in each figure) did not change; however, the fraction of the organic crystals decreased to 18%, compared with those precipitated without $FeCl_3$. This is due to the increased solubility brought about by the addition of the $FeCl_3$ solution and the ionic strength of the Fe^{III} ions [19]. In addition, although it is known that there exist different crystal polymorphs of organic crystals depending on the crystallization temperature and solvent composition [20], however, structural change was not observed in our experimental conditions.

OM images of the organic crystals and SEM images of the corresponding replicated PPy microstructures synthesized by the above process are shown in Figs. 3 and 4, respectively. As the K^+ ion of 4-SBAK was substituted with Na^+ (4-SBANa) and Li^+ (4-SBALi), the shape of the organic crystals changed from hexagonal microplates (Fig. 3a) to long needles (Fig. 3b) and lozenge-shaped microplates (Fig. 3c), respectively. Moreover, as the position of the sulfonate group in the benzene ring shifted from *para*-(4-SBAK) to *meta*-(3-SBANa) and *ortho*-(2-$SBANH_4$), the shape of the organic crystals changed to rigid rods (Fig. 3d) and parallelogram microplates (Fig. 3e).

The 4-SBAK crystals (Fig. 3a) that precipitated in an aqueous KCl solution exhibited hexagonal microplate shapes, leading to the formation of similarly shaped PPy hexagonal microplates about 75 μm long and 25 μm wide (Fig. 4a). A close look at the surface of PPy hexagonal microplate indicated that the smooth PPy surface consisted of granular nanoparticulates (Fig. 4a, inset). In the case of the long needlelike crystals of 4-SBANa (Fig. 3b), the morphology of the polymerized PPy changed significantly, mimicking the original shape of the 4-SBANa crystals; instead of micro-sized long needles, entangled PPy nanofibers resulted (Fig. 4b). SEM images at higher magnifications (Fig. 4b, inset) revealed that the nanofibers had diameters of 300–500 nm and lengths varying from tens to hundreds of micrometers. Similarly, the existence of differently shaped organic crystals, such as lozenge-like crystals of 4-SBALi (Fig. 3c), rigid-rod 3-SBANa crystals (Fig. 3d), and 2-$SBANH_4$ parallelogram crystals (Fig. 3e), in the polymerization medium produced shaped-matched PPy structures. A lozenge-shaped PPy microplate of about 10 μm in width (Fig. 4c), rigid rod-type PPys of

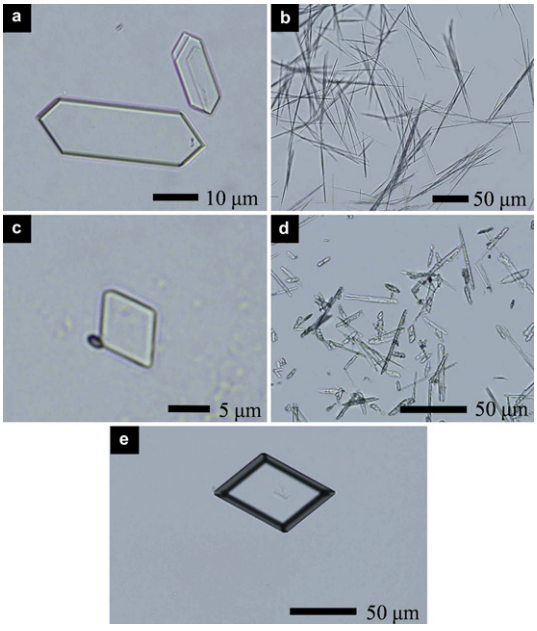

Fig. 3. OM images of (a) 4-SBAK, (b) 4-SBANa, (c) 4-SBALi, (d) 3-SBANa, and (e) 2-$SBANH_4$ organic crystals before polymerization.

50–80 μm in length (Fig. 4d and inset), and a parallelogram-shaped PPy microplates of about 25–30 μm in width (Fig. 4e) are shown in Fig. 4c–e. Similarly to the PPy hexagonal microplates, the surface of the PPys polymerized with 4-SBALi and 2-SBANH$_4$ crystals consisted of granular nanoparticles (Fig. 4c, inset, and Fig. 4e, inset). This is a general phenomenon that has been reported in previous reports describing the PPy structures [14,15,19]. It is thought that heterogeneous nucleation of cationic PPy chains on anionic organic crystal surfaces produced the interconnected spherical nanoparticles of PPy microstructures. For comparison, conventional PPy that was polymerized in the absence of organic crystals showed agglomerates of 200–500-nm spherical nanoparticles (Fig. 4f and inset) instead of microstructures. The results shown in Figs. 3 and 4 demonstrate that the organic crystals acted as sacrificial templates during PPy growth, allowing PPy to copy the shapes of the precipitated organic crystals. Moreover, while the polymerization yield of conventional PPy was as low as 25.6%, the yield of PPy produced in the presence of organic crystals as sacrificial templates was 45.7–49.1% regardless of organic salts (Table 1).

As reported in our previous work [19], the presence of the relevant organic crystals is essential for the formation of the shape-copied PPy microstructures. A schematic diagram illustrating the formation process is presented in Fig. 5a. First, organic crystals are precipitated by recrystallization below the saturation temperature in an aqueous inorganic salt medium. Upon initiation of the PPy polymerization, the anionic surfaces of the organic crystals are increasingly covered with growing cationic PPy via electrostatic interactions. The organic crystals would separate from the PPy microstructures by both continuous dissolution and fragmentation of the organic crystals, resulting from the addition of an oxidant solution and mechanical stirring. Finally, shape-copied PPy microstructures are formed. The electrostatic interactions [21,22] between growing cationic PPy chains and anionic surfaces of organic crystals during the polymerization drive the PPy replication of the organic crystal templates (Fig. 5b). Experimental evidence of the binding of PPy on the crystal surface is shown in Fig. 5c and d. The 4-SBAK crystal surface prior to PPy synthesis remained smooth (Fig. 5c), whereas nucleation of PPy (white spots, 100–200 nm in size) was observed on the 4-SBAK crystal surface through electrostatic interaction after a synthesis time of 10 min (Fig. 5d).

For additional experimental evidence, zeta potentials were measured for the organic crystals and the conventional PPy

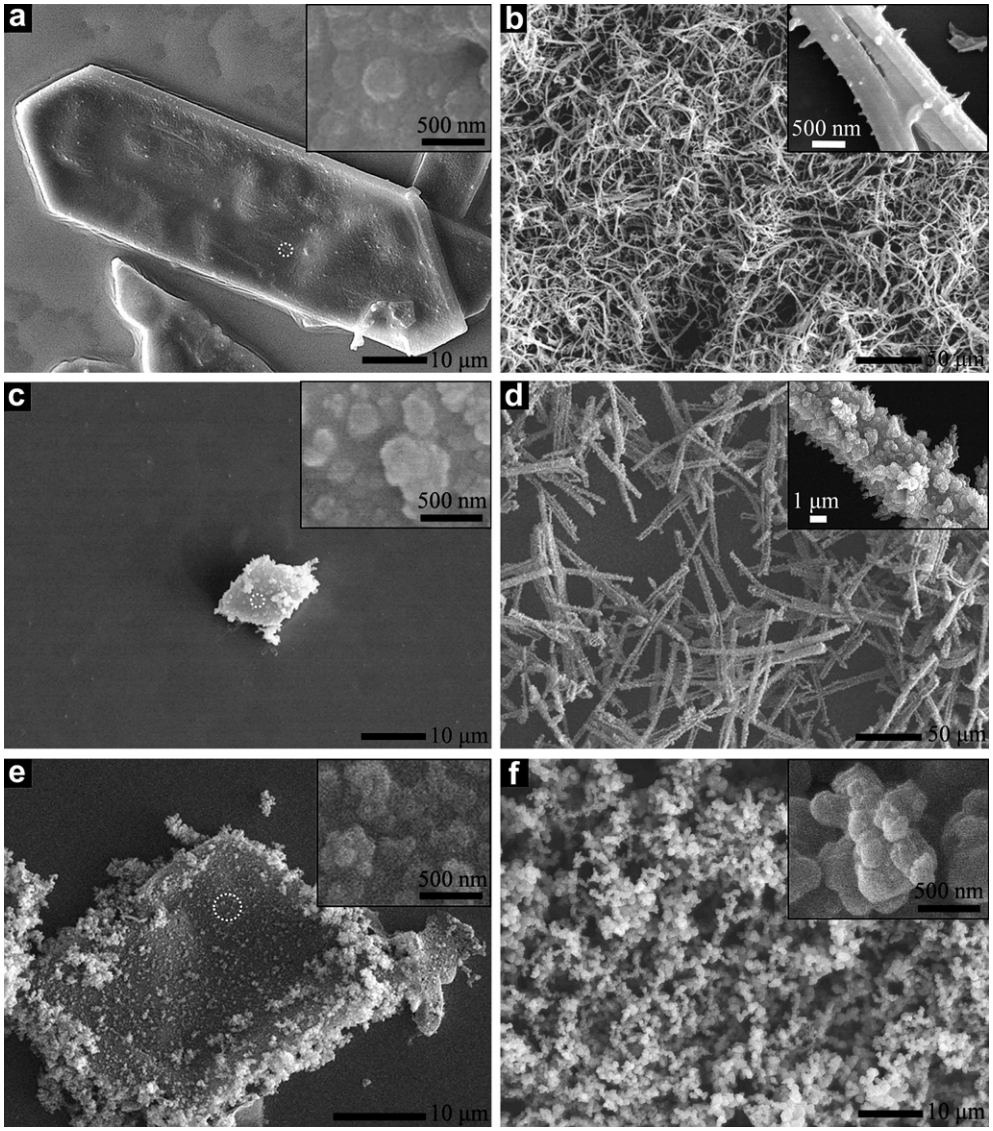

Fig. 4. SEM images of PPys polymerized in the presence of (a) 4-SBAK, (b) 4-SBANa, (c) 4-SBALi, (d) 3-SBANa, and (e) 2-SBANH$_4$ crystals. (f) SEM image of the conventional PPy. The insets in (a), (c), and (d) show the magnified images of the circle in images and the insets in (b), (d), and (f) show the magnified images of the PPys, respectively.

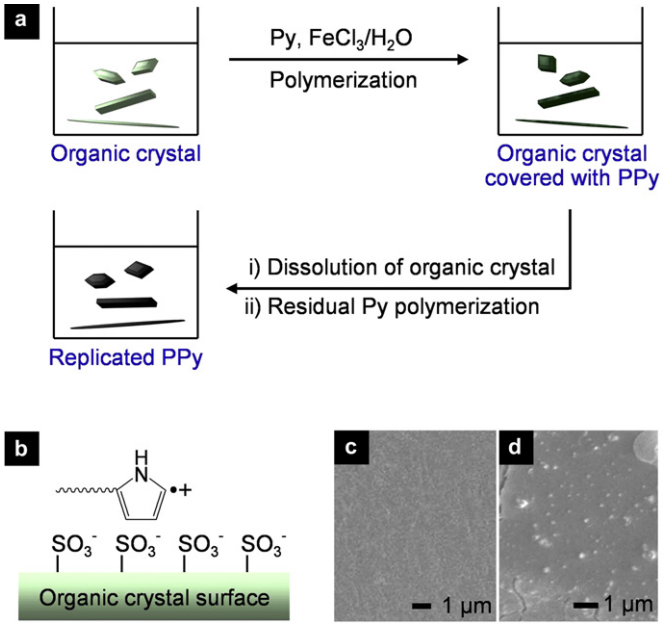

Fig. 5. (a) Schematic diagram of the organic crystal-directed fabrication of PPy microstructures. (b) A simplified illustration of the electrostatic interaction between growing radical cationic PPy chains and anionic crystal surfaces. SEM images of (c) 4-SBAK crystal surface before polymerization and (d) PPy nucleation on the 4-SBAK crystal surface by electrostatic interaction at polymerization time of 10 min.

obtained at a polymerization time of 10 min (Table 2). For the organic crystals, regardless of the organic salt molecules, negative zeta potentials (surface charge) were observed ranging from −1.77 to −2.18 mV. In contrast, the zeta potential for the conventional PPy produced at a polymerization time of 10 min had a positive value, +32.4 mV, indicating the formation of PPy radical cations during polymerization. The cationic PPy chains are adsorbed on the anionic surfaces of the organic crystals through electrostatic interactions, generating nucleation sites for subsequent polymerization reactions. Thus, the zeta potential measurement provides further evidence that the cationic PPy chains grew from the anionic surfaces of the organic crystals.

FT-IR spectra (Fig. 6) of the PPys fabricated by the organic crystal-mediated method were essentially identical to that of the conventional PPy [23,24]. All characteristic bands of PPy, such as the peaks at around 1560 and 1480 cm^{-1} assigned to the antisymmetric ring stretching mode and symmetric mode in the Py ring, the peaks at 1042 and 1318 cm^{-1} attributed to C–H and N–H deformation vibration modes, and the peaks at around 1175 and 900 cm^{-1}, which correspond to the C–H vibration mode in the Py rings, were observed from the resultant microstructures. These spectral characteristics indicate that PPy was successfully polymerized in the presence of the organic crystals.

Bulk *I*–*V* behaviors of the PPys (pressed pellets) were measured, as shown in Fig. 7. The PPy microstructures exhibited

Table 2
Zeta potentials of the organic crystals and PPy dispersions.

Samples	Zeta potential (mV)
4-SBAK	−2.09
4-SBANa	−2.14
4-SBALi	−1.77
3-SBANa	−1.84
2-$SBANH_4$	−2.18
PPy-10[a]	+32.4

[a] PPy after washing at a polymerization time of 10 min.

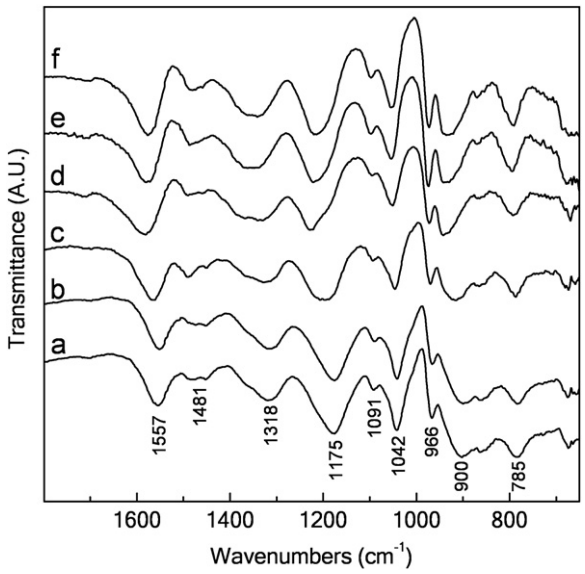

Fig. 6. FT-IR spectra of the PPys. (a), (b), (c), (d), and (e) PPy synthesized in the presence of organic crystals of 4-SBAK, 4-SBANa, 4-SBALi, 3-SBANa, and 2-$SBANH_4$, respectively; (f) conventional PPy.

semiconductivity [25]. The bulk *I*–*V* curves of the semiconducting PPy showed breakdown voltages. To obtain the breakdown voltages of the bulk PPys, the d*I*/d*V* signals were taken from the *I*–*V* curves, as shown in Fig. 7 (inset). The d*I*/d*V* signals of the PPys with high conductance polymerized in the presence of 4-SBAK, 4-SBANa, and 4-SBALi crystals had relatively lower breakdown voltages (2.3–2.5 V) than that of the conventional PPy (4.4 V). In contrast, the breakdown voltages of the PPys polymerized in the presence of 3-SBANa or 2-$SBANH_4$ were beyond the measured voltage range. Moreover, the conductance of PPy samples polymerized in the presence of 3-SBANa or 2-$SBANH_4$ was markedly reduced. The *I*–*V* data corresponded well with the conductivity data (Table 3). However, the conductivity of the PPy microstructures varied widely from 10^{-1} to 10^{2} Scm^{-1}, depending on the type of the organic salt molecules. The reason for this will be explained later.

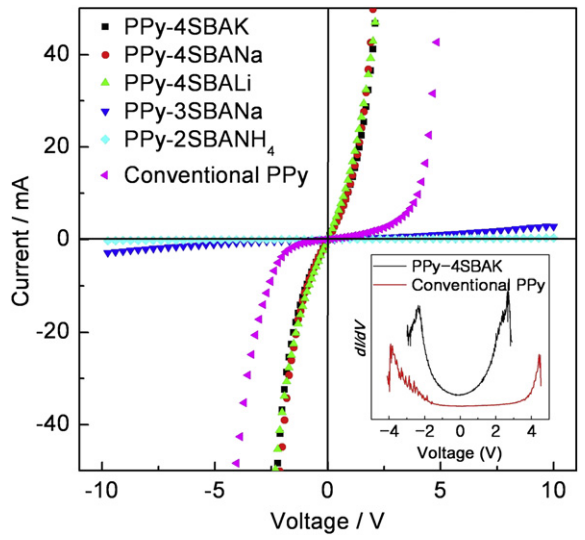

Fig. 7. *I*–*V* curves for the PPys. The inset graph shows the d*I*/d*V* signals obtained from the *I*–*V* curves of PPy-4SBAK and conventional PPy.

Table 3
Properties of PPys obtained at various conditions.

Samples	N^+/N ratio[a]	XRD peak analysis		Conductivity (Scm^{-1})
		$2\theta(001)$ (deg)	d(001) (Å)	
PPy-4SBAK	0.28	26.4	3.38	200.3
PPy-4SBANa	0.25	26.1	3.41	168.2
PPy-4SBALi	0.23	25.8	3.45	117.5
PPy-3SBANa	0.20	25.3	3.52	17.2
PPy-2SBANH$_4$	0.15	23.3	3.82	0.8
Conventional PPy	0.28	25.3	3.52	33.7

[a] Ratio of the N^+ components to the total area of the N1s peak.

The XPS nitrogen 1s (N 1s) core level spectra of the various PPys at room temperature are shown in Fig. 8. The main peak component at about ~399.8 eV is attributable to neutral amine nitrogen (−NH−) in the pyrrole ring [26,27]. However, this peak is not symmetric. The low binding energy component of shoulder peak at about ~397.9 eV is assigned to the imine nitrogen (−N=) [26,27]. The high binding energy shoulder, which was deconvoluted into two peaks at about 401.2 and 402.8 eV, can be defined as positively charged nitrogens of (N^+) in the pyrrole ring, such as $-NH^+-$ and $-N^+=$, respectively [27,28]. Based on the information obtained from the XPS N 1s spectra, protonation levels on the nitrogen sites can be determined in terms of N^+/N_{total} [27,28]. The N^+/N_{total} ratio is nearly consistent with the doping level because the doped anions are ideally balanced by the positive charges in the pyrrole rings. The N^+/N_{total} ratios of the PPys polymerized with 4-SBAK, 4-SBANa, 4-SBALi, 3-SBANa, and 2-SBANH$_4$ were 28.0, 25.0, 23.1, 20.3, and 14.6%, respectively. This data correlated well with the conductivity

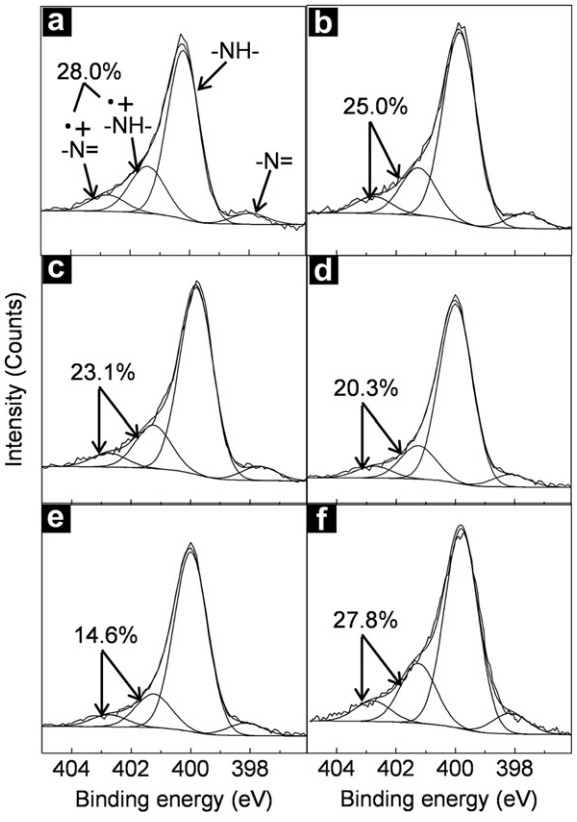

Fig. 8. Nitrogen 1s (N 1s) XPS core level spectra of the PPys. (a), (b), (c), (d), and (e) PPy synthesized in the presence of 4-SBAK, 4-SBANa, 4-SBALi, 3-SBANa and 2-SBANH$_4$ crystals, respectively; (f) conventional PPy.

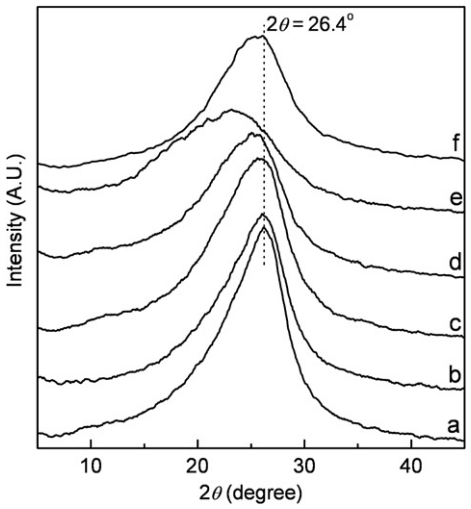

Fig. 9. XRD patterns of the PPy. (a), (b), (c), (d), and (e) PPy synthesized in the presence of of 4-SBAK, 4-SBANa, 4-SBALi, 3-SBANa and 2-SBANH$_4$ crystals, respectively; (f) conventional PPy.

data (Table 3). Generally, as the doping level increases, conductivity increases, but the result of the conventional PPy was somewhat inconsistent with those of PPys polymerized with organic crystals. Although the N^+/N_{total} ratio of the conventional PPy was very high, up to 27.8%, similar to that of the PPy polymerized with 4-SBAK crystals, the conductivity was as low as 33 Scm^{-1}. Additionally, as the K^+ ion of 4-SBAK was substituted with Na^+ and Li^+ and the position of the sulfonate group on the benzene ring shifted from *para* to *meta* and *ortho*, the N^+/N_{total} ratios decreased with decreasing conductivity. In this experiment, another factor governing the electrical property of PPys appeared to be the degree of structural order. Thus, we suggest that the degree of π-stacking and average face-to-face distance of the π-stacked inter-Py rings may be partially responsible for the widely different electrical properties of the PPys.

XRD patterns of the PPys polymerized in the presence of organic crystals and conventional PPy are shown in Fig. 9. The peak at around 26.4° is associated with the average π-stacking distance (d_{001}) of the inter-Py rings [19,29]. The π-stacking of aromatic rings in PPy chains is influenced by the structures of the aromatic planar molecules, such as aromatic sulfonic acid salts used in this study that can be crystallized by π-stacking. The enhanced π-stacking- and decreased π-stacking-distance between PPy rings improved the conductivity [19,30,31]. As the position of the sulfonate group on the benzene ring shifts from *para* (Fig. 9a–c) to *meta* (Fig. 9d) and *ortho* (Fig. 9e), effective π-stacking of the Py rings was interrupted by the steric effect between the carboxyl and sulfonate groups. Thus, as shown in Table 3, the peak at around 26.4° shifted toward the lower angle for the PPys from 3-SBANa and 2-SBANH$_4$ ($2\theta \approx 25.3°$ and 23.3°, respectively), and the *d*-spacing of the (001) plane increased from 3.38 to 3.82 Å, accompanied by peak broadening and reduced intensity. As a result, the conductivity of the PPys decreased due to the structural imperfections arising from the inefficient π-stacking and the interruption of the effective interchain charge transport brought by the increased π-stacking distance. Additionally, the XRD pattern of the conventional PPy also exhibited reduced intensity and lower 2θ peak position ($2\theta \approx 25.3°$ ($d_{001} = 3.52$ Å)) compared to the PPy polymerized in the presence of the 4-SBAK crystals at a similar doping level, which correlated with the conductivity data. Considering the results of Table 3, the electrical properties of the synthesized PPys are likely governed not only by the N^+/N_{total} ratio related to doping level but also by the

structural difference brought about by different synthetic routes and structures of the organic salt molecules used. Further experiments to understand the difference in conductivity of the PPys polymerized with the 4-SBAK, 4-SBANa, and 4-SBALi crystals are currently under investigation.

4. Conclusion

In summary, various conducting PPy microstructures were synthesized using the proposed organic crystal-directed fabrication method. Our facile approach has the following advantages: i) the morphologies of the resultant PPy are controlled by the shapes and sizes of the organic crystals, ii) the automatic template removal and self-assembly processes occur concurrently in one pot, and iii) the electrical properties and structural order of the resultant PPy can be altered by the chemical structure of the organic molecules forming the crystals. This approach should provide a general method for shaped-controlled fabrication of a conducting polymer such as polyaniline with different micro/nanostructures. With the organic crystal template in a monodispersed nanometer-sized form, the resulting conducting polymer should be reproduced in the same size and shape of the template crystal, which would have great potential applications in plastic electronics, such as sensors, electrodes, field effect transistors, and substitutes for carbon materials.

Acknowledgements

This work was supported by Basic Science Research Program through the National Research Foundation of Korea (NRF) grant funded from the Ministry of Education, Science and Technology (MEST) of Korea for the Center for Next Generation Dye-sensitized Solar Cells (No. 2010-0001842) and research fund of Hanyang University (HYU-2010-T).

References

[1] Wu CG, Bein T. Science 1994;264:1757.
[2] Martin CR. Chem Mater 1996;8:1739.
[3] Jang J, Oh JH. Chem Commun; 2004:882.
[4] Han MG, Foulger SH. Small 2006;2:1164.
[5] Huang LM, Wang ZB, Wang HT, Cheng XL, Mitra A, Yan YS. J Mater Chem 2002;12:388.
[6] Jang J, Yoon H. Chem Commun; 2003:720.
[7] Wei Z, Zhang Z, Wan M. Langmuir 2002;18:917.
[8] Zhang Z, Wei Z, Wan M. Macromolecules 2002;35:5937.
[9] Kim BJ, Oh SG, Han MG, Im SS. Langmuir 2000;16:5841.
[10] Choi JW, Han MG, Kim SY, Oh SG, Im SS. Synth Met 2004;141:293.
[11] Jang J, Oh JH. Adv Funct Mater 2005;15:494.
[12] Jang J, Yoon H. Small 2005;1:1195.
[13] Yang X, Zhu Z, Dai T, Lu Yun. Macromol Rapid Commun 2005;26:1736.
[14] Yan W, Han J. Polymer 2007;48:6782.
[15] Diez I, Tauer K, Schulz B. Colloid Polym Sci 2006;284:1431.
[16] Dai T, Lu Y. Macromol Rapid Commun 2007;28:629.
[17] Wang Y, Chen W, Zhou D, Xue G. Macromol Chem Phys 2009;210:936.
[18] Wang Y, Yu C, Li Z, Zhou D, Chen W, Xue G. Colloid Polym Sci 2009;287:1325.
[19] Jeon SS, Park JK, Yoon CS, Im SS. Langmuir 2009;25:11420.
[20] Kariuki BM, Jones W. Acta Cryst 1995;C51:867.
[21] He YH, Yuan JY, Shi GQ. J Mater Chem 2005;15:859.
[22] Beadle PM, Armes SP, Greaves SJ, Watts JF. Langmuir 1996;12:1784.
[23] Omastová M, Trchová M, Kovářová J. Stejskal J Synth Met 2003;138:447.
[24] Li X, Wan M, Wei Y, Shen JY, Chen ZJ. J Phys Chem B 2006;110:14623.
[25] Lee HJ, Park SM. J Phys Chem B 2004;108:1590.
[26] Idla K, Talo A, Niemi HE-M, Forsen O, Ylasaari S. Surf Interface Anal 1997;25:837.
[27] Zhang X, Bai RB. Langmuir 2002;18:3459.
[28] Joo J, Lee JK, Lee SY, Jang KS, Oh EJ, Epstein AJ. Macromolecules 2000;33:5131.
[29] Geiss RH, Street GB, Volksen W. Economy J. IBM J Res Dev 1983;27:321.
[30] Wynne KJ, Street GB. Macromolecules 1985;18:2361.
[31] Warren MR, Madden JD. Synth Met 2006;156:724.